Journal of Alloys and Compounds 509 (2011) 1705–1710

Contents lists available at ScienceDirect

Journal of Alloys and Compounds

journal homepage: www.elsevier.com/locate/jallcom

Dielectric relaxation and conduction mechanism in $LaNi_{3/4}M_{1/4}O_3$ (M = Mo, W) at low temperature

Alo Dutta*, T.P. Sinha

Department of Physics, Bose Institute, 93/1 Acharya Prafulla Chandra Road, Kolkata 700009, West Bengal, India

ARTICLE INFO

Article history:
Received 19 July 2010
Received in revised form 6 October 2010
Accepted 7 October 2010
Available online 14 October 2010

Keywords:
Ceramic
Solid state reaction
Electrical transport
X-ray diffraction

ABSTRACT

In order to investigate the electrical transport in $LaNi_{3/4}Mo_{1/4}O_3$ and $LaNi_{3/4}W_{1/4}O_3$, the dc conductivity and dielectric properties in these polycrystalline materials are investigated in the temperature range from 163 K to 383 K and frequency range from 50 Hz to 1 MHz. The X-ray diffraction patterns of the samples show monoclinic phase at room temperature. The homogeneity of the samples is determined by energy dispersive analysis of X-ray (EDAX) attached with a scanning electron microscope. The temperature dependence of dc conductivity shows the semiconducting nature of the materials. The complex impedance plane plots show that the relaxation (conduction) mechanism in these materials is purely a bulk effect arising from the semiconductive grains. The frequency-dependent electrical data are also analyzed in the framework of ac conductivity formalism. The ac conductivity spectra follow the universal power law. The activation energies required for bulk conduction is 0.143 and 0.165 eV for LNM and LNW respectively. The scaling behaviour of loss tangent suggests that the relaxation describes the same mechanism at various temperatures.

1. Introduction

Perovskite oxides with high dielectric constant play an important role in microelectronics [1], and have been used as memory devices and capacitors. In the literature, the dielectric relaxation with extremely high permittivity has been reported in many materials, in which the contribution of conduction carriers (electrons, holes, ions, polarons and protons) to dielectric polarization may play an important role. However, the explanation of this phenomenon is controversial based on different models [2–5]. The electron localized on an ion (or a few ions) can cause displacements of neighbouring ions from their positions in the crystal lattice. The quasiparticle formed by an electron and corresponding lattice displacements is called polaron [6–8]. The polaron is a small polaron if the electron is localized mostly on one ion or an intermediate polaron if localized on a group of ions. We reserve the term large polaron for a delocalized polaron which is an electron moving together with polarization of the surrounding medium.

Low frequency dielectric relaxation behaviour observed in numerous perovskite oxides is not related to a phase transition, and probably related to a series of excitations in the solid [9]. Iguchi et al. reported polaronic conduction in n-type $BaTiO_3$ doped with La_2O_3 or Gd_2O_3 accomplished by a low frequency dielectric loss dispersion with the activation energy of 0.068 eV, which were explained as being due to the hopping motion of non-adiabatic small polarons [9]. However, due to the complicated characteristics of the real materials including the lattice contribution, different defects, impurities and coupling effects, a uniform explanation concerning the low-frequency dielectric relaxation behaviour is difficult and needs firmer experimental basis to be accomplished. Detailed studies are therefore needed to shed light on the physical nature of these phenomena, and more experimental data in different systems are also required.

In this work we study the electrical conduction mechanism in two La-based materials, $LaNi_{3/4}Mo_{1/4}O_3$ (LNM) and $LaNi_{3/4}W_{1/4}O_3$ (LNW) at low temperature. Arima and Tokura [10] studied the optical conductivity of $LaNiO_3$ and concluded the metallic nature of $LaNiO_3$ due to the absence of any charge gap in the conductivity spectrum. In this study we have made an attempt to investigate the changes in the transport properties of the parent compound $LaNiO_3$ by doping the two transition metals Mo and W separately in the B-site. In strongly correlated system, polaronic conduction plays an important role in electrical transport. Though, there are many means to address polaron dynamics in perovskite oxides, dielectric properties can also provide important information, because there is a high probability of a hopping process for polarons to result in a dielectric relaxation [11–14]. If a hoping process of small polarons dominates in the electrical transport at low temperature in various oxides [15–19], dielectric measurements on these materials would be very important in the investigation of polaron dynamics.

* Corresponding author. Tel.: +91 033 23031189; fax: +91 033 23506790.
E-mail address: alo.dutta@yahoo.com (A. Dutta).

0925-8388/$ – see front matter © 2010 Elsevier B.V. All rights reserved.
doi:10.1016/j.jallcom.2010.10.012

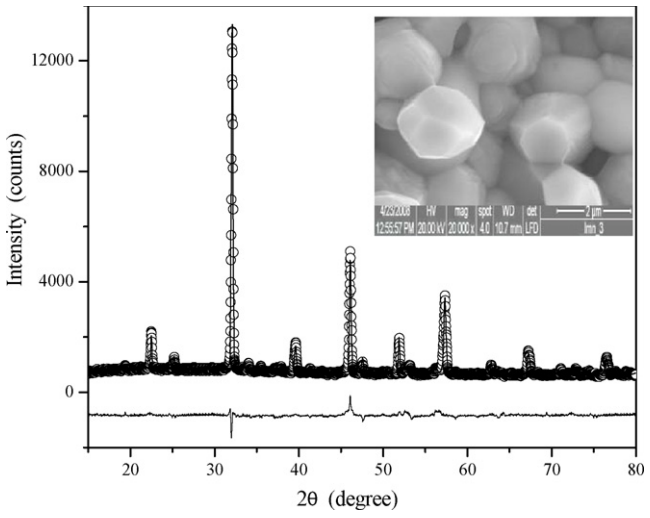

Fig. 1. XRD pattern of $LaNi_{3/4}Mo_{1/4}O_3$ at room temperature. The SEM is shown in the inset.

2. Experimental

In analogy to our previous work [20–23], the solid state reaction technique was employed for the synthesis of LNM and LNW. The powders of La_2O_3, $NiCO_3$, MoO_3 and WO_3 were taken in stoichiometric ratio and mixed in the presence of acetone for 12 h. The mixture was calcined at 1350 °C in air for 8 h and brought to room temperature at the cooling rate of 100 °C/h. The calcined samples were pelletized into a disc using polyvinyl alcohol as binder. Finally, the discs were annealed at the temperature 1050 °C for 10 h and cooled down to room temperature by adjusting the cooling rate (30 °C/h).

The determination of lattice parameters and the identification of the phases were carried out using an X-ray powder diffractometer (Rigaku Miniflex II). The X-ray diffraction (XRD) patterns were collected in the 2θ range, 10–80° by step scanning at 0.02° per step at room temperature. The homogeneity of the samples was determined by energy dispersive analysis of X-ray (EDAX) attached with a FEI Quanta 200 scanning electron microscope (SEM). The infrared (IR) spectra of the samples were recorded between 350 and 2000 cm^{-1} with a Perkin-Elemer FT-IR instrument, using the KBr pellet technique.

The samples prepared for electrical measurements were polished. Silver electrodes were formed onto both sides of the disc by using silver paste and fired. The capacitance and conductance were measured by using an LCR meter (HIOKI) in the frequency range from 50 Hz to 1 MHz and in the temperature range from 163 K to 383 K.

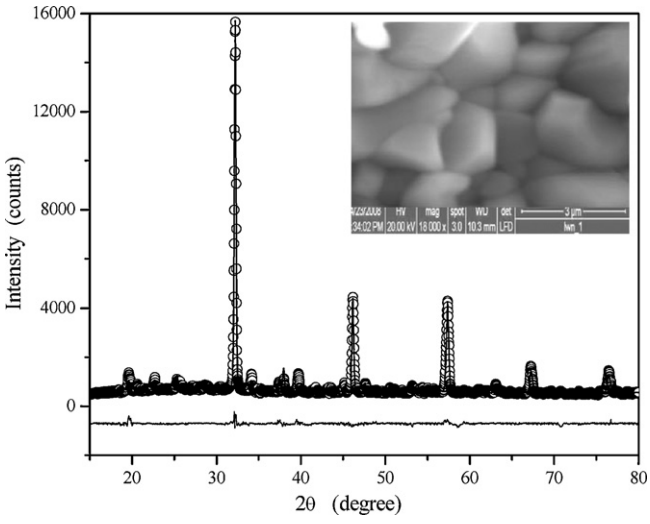

Fig. 2. XRD pattern of $LaNi_{3/4}W_{1/4}O_3$ at room temperature. The SEM is shown in the inset.

Table 1
Rietveld refinement parameters from XRD analysis of the samples.

Materials	Lattice parameters	R_P	WR_P	χ^2
$LaNi_{3/4}Mo_{1/4}O_3$	$a = 5.58$ Å, $b = 5.59$ Å, $c = 7.88$ Å, $\beta = 90.11°$	6.8%	10%	7.6
$LaNi_{3/4}W_{1/4}O_3$	$a = 5.59$ Å, $b = 5.61$ Å, $c = 7.90$ Å, $\beta = 89.90°$	7.4%	10%	7.9

3. Results and discussion

3.1. Structural study

The X-ray diffraction patterns of LNM and LNW are shown in Figs. 1 and 2 respectively. The XRD data of the samples are subjected to Rietveld refinement with space group $P2_1/n$ (monoclinic) by using GSAS code and corresponding structural data are listed in Table 1. The continuous lines in Figs. 1 and 2 show the Rietveld fitting of the XRD data. The quantity of fit and the absence of any unaccounted diffraction peak indicate that the synthesized samples have single phase.

SEM images of the samples are shown in the inset of Figs. 1 and 2 for LNM and LNW respectively. The SEM images indicate the uniformity of the grains in the samples. The average grain size of LNM is 1.74 μm and LNW is 1.46 μm. The survey spectrum obtained by EDAX is shown in Fig. 3. Well resolved lines originating from the constituent atoms are recorded in the energy range of 0–10 keV. The EDAX spectrum confirms the homogeneity and the absence of any impurity in the samples.

Fig. 4 shows the FT-IR spectrum of LNM and LNW. Both the materials exhibit six main vibrational modes in the 350–2000 cm^{-1} range. All the peaks in the spectra are the characteristics of the materials. The two absorption bands appearing in between 390 and 490 cm^{-1} are due to the NiO_6 octahedra where the lower and higher wavenumber bands are assigned for the bending and stretching mode of Ni–O bond respectively. The strong absorption peak at around 600 cm^{-1} is assigned for La–O stretching vibrational mode in both the materials. The absorption peaks corresponding to Mo–O and W–O vibrational modes appear in between 760 and 860 cm^{-1} for LNM and LNW respectively. The absorption band around 760 cm^{-1} may appear due to the bending vibra-

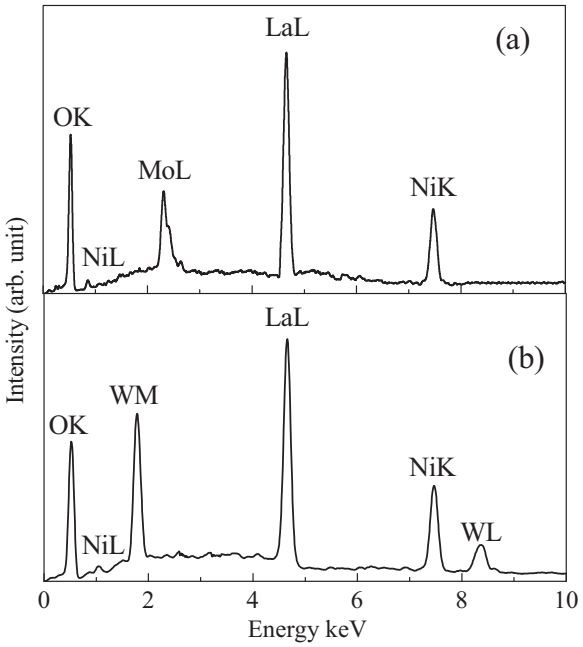

Fig. 3. Survey spectrum of EDAX for $LaNi_{3/4}Mo_{1/4}O_3$ (a) and $LaNi_{3/4}W_{1/4}O_3$ (b).

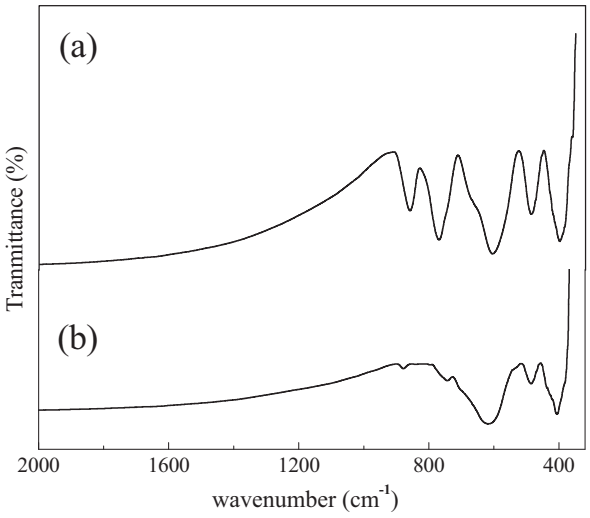

Fig. 4. FT-IR spectrum of $LaNi_{3/4}Mo_{1/4}O_3$ (a) and $LaNi_{3/4}W_{1/4}O_3$ (b).

tional mode of the corresponding oxygen polyhedra whereas the band around 860 cm^{-1} is assigned for the asymmetric stretching mode of the same oxygen polyhedra in the corresponding materials.

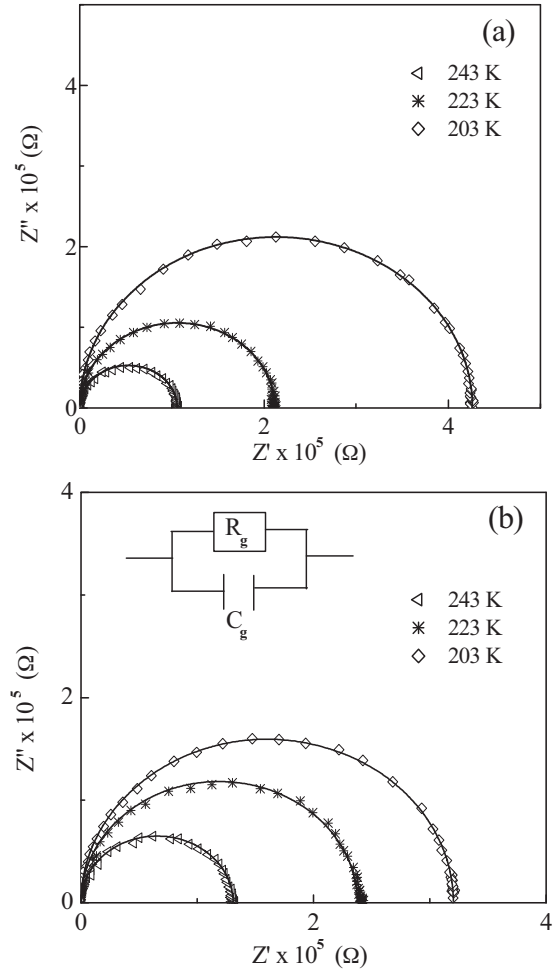

Fig. 5. Complex plane impedance plots for $LaNi_{3/4}Mo_{1/4}O_3$ (a) and $LaNi_{3/4}W_{1/4}O_3$ (b) (solid lines are the fitting to the data by the RC equivalent circuit).

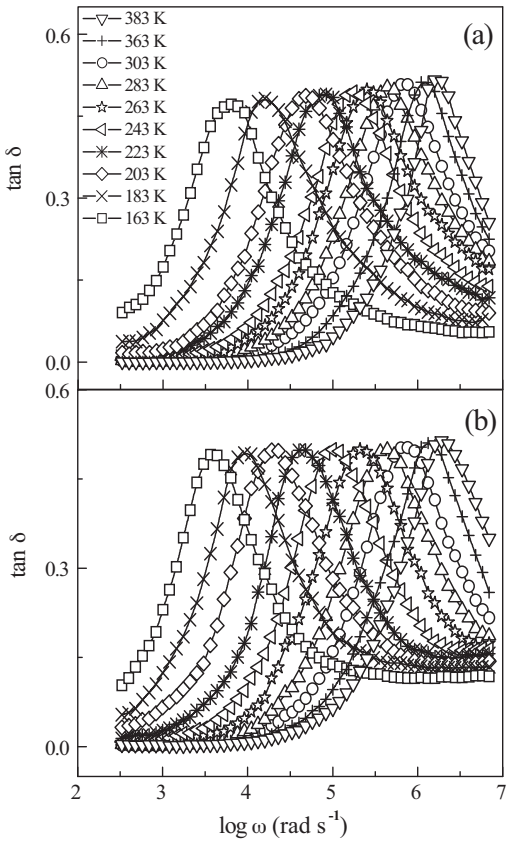

Fig. 6. Frequency dependence of the tan δ of $LaNi_{3/4}Mo_{1/4}O_3$ (a) and $LaNi_{3/4}W_{1/4}O_3$ (b) at various temperatures.

3.2. Complex impedance analysis

Usually, in polycrystalline ceramics, three independent semicircular arcs are obtained in the complex impedance plane plots where the real part (Z') of the total impedance is plotted against the imaginary part (Z'') as a parametric function of frequency, i.e., the highest-frequency arc is attributed to the bulk conduction, the intermediate frequency arc is due to the grain-boundary conduction, and the lowest frequency arc corresponds to the transport across the electrode–specimen interface. Fig. 5 shows the complex impedance plane plots for LNM and LNW in the temperature range from 203 K to 243 K. At all temperatures the presence of single arc passing through the origin in the high frequency side for both the cases indicates that the conduction mechanism in these materials corresponds to the bulk effect arising in semiconductive grains. These arcs can be explained by the electrical equivalent circuit consisting of a parallel combination of bulk resistance (R_g) and bulk capacitance (C_g). We have fitted our experimental data at three different temperatures for both the materials with the single RC equivalent circuit (inset of Fig. 5) as defined by the following equations:

$$Z^* = Z' + Z'' = \frac{1}{R_g^{-1} + j\omega C_g};$$
$$Z' = \frac{R_g}{1+(\omega R_g C_g)^2}; Z'' = R_g\left[\frac{\omega R_g C_g}{1+(\omega R_g C_g)^2}\right] \quad (1)$$

The solid lines in Fig. 5 are the best fittings of Eq. (1). No residual semicircle at intermediate and/or low frequencies attributed to grain boundary and/or electrode effects has been observed.

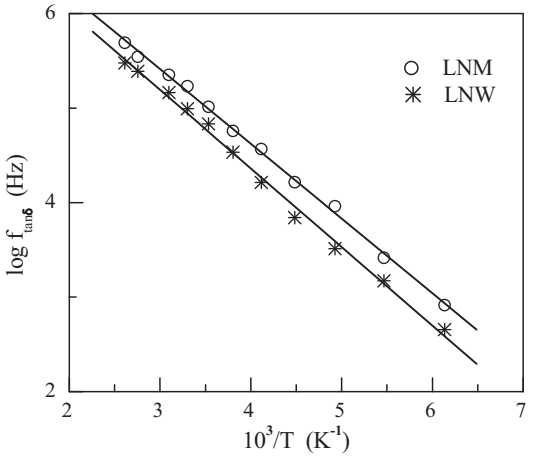

Fig. 7. The temperature dependence of $f_{\tan\delta}$ for $LaNi_{3/4}Mo_{1/4}O_3$ and $LaNi_{3/4}W_{1/4}O_3$.

3.3. Dielectric relaxation

Fig. 6 shows the angular frequency ($\omega = 2\pi f$) dependence of loss tangent ($\tan\delta$) as a function of temperature. At each temperature, the spectrum involves a dielectric relaxation process possessing the maximum loss factor, $\tan\delta_m$ at the resonance frequency $f_{\tan\delta}$. As temperature increases, the resonance frequency regularly increases like dielectric relaxation caused by a hopping process of small polarons in other transition metal oxides [24,25]. The emergence of such a dielectric relaxation process in the ac measurements certainly ensures that the hopping conduction of small polarons takes place in these materials.

In the dielectric materials if the relaxation process arises due to the polaronic conduction, the relaxation phenomenon can be described by Debye's theory [26]. In such cases the temperature dependence of resonance frequency corresponding to loss tangent satisfies the Arrhenius law. The relaxation (resonance) frequency is proportional to $\exp(-Q/k_BT)$, Q being the activation energy required for the relaxation mechanism. In the case of dielectric relaxation due to a small polaron hopping process, the relation between activation energy and the hopping energy (ω_H) is $Q = (\omega_H + \omega_D/2)$, where ω_D is the disordered energy [27]. The Arrhenius relation of $f_{\tan\delta}$ is shown in Fig. 7. The hopping energies as obtained from the linear fit to the experimental data points are 0.143 eV and 0.165 eV for LNM and LNW respectively.

3.4. dc and ac conductivity

In case of small polaron hopping process, the temperature dependence of dc conductivity can be expressed as [15–17,27–33]:

$$\sigma_{dc} = \frac{n_0 a^2 e^2 \omega_{LO}}{k_B T} \exp\left[-\frac{\omega_H + E_g/2 + \omega_D/2}{k_B T}\right] = \frac{A}{T} \exp\left[-\frac{\omega_H + E_g/2 + \omega_D/2}{k_B T}\right] \quad (2)$$

where e denotes the electronic charge, $n_0 \exp(-E_g/2k_BT)$ is the number of small polaron per unit volume, a is the characteristic intersite hopping distance, ω_{LO} is the optical phonon frequency and E_g is the band gap energy. Fig. 8 shows the temperature dependence of dc conductivity of these materials. The dc activation energies as obtained from the linear fit of the experimental data in Fig. 8 are 0.157 eV and 0.192 eV for LNM and LNW respectively. The experiment cannot separate $(\omega_H + \omega_D/2)$ into individuals, but as suggested by Dominik and MacCrone [34] and later confirmed by Jung, Iguchi and their co-workers [9,31,35] that the disordered energy is generally negligibly small compared with ω_H, even less than the experimental error in the determination of ω_H for the bulk conduction in crystalline materials and hence can be omitted in Eq. (2). In such situation the band gap energy can be calculated from the difference between the dc activation energy and hopping energy of small polaron. The band gap energies for LNM and LNW are 0.028 eV and

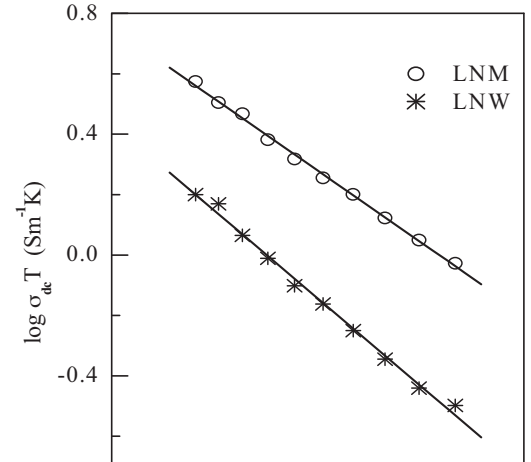

Fig. 8. Temperature dependence of dc conductivity of $LaNi_{3/4}Mo_{1/4}O_3$ and $LaNi_{3/4}W_{1/4}O_3$.

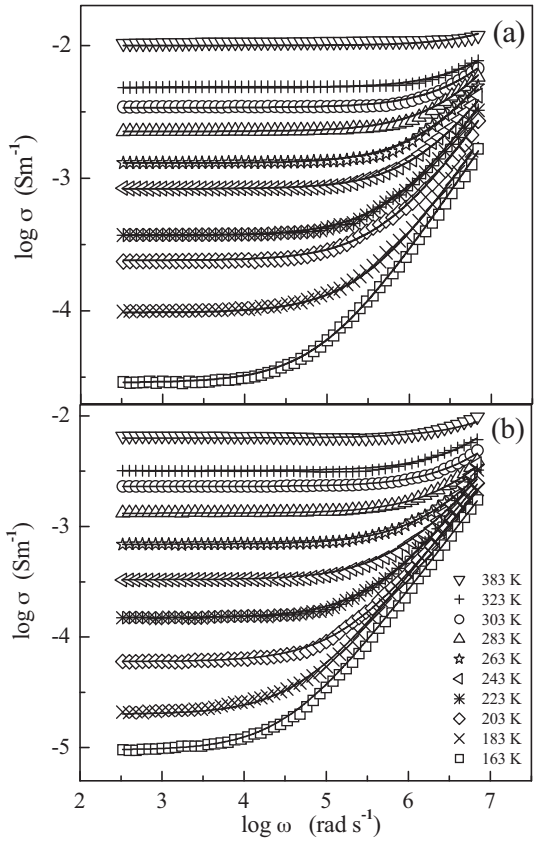

Fig. 9. Frequency dependence of the ac conductivity (σ) for $LaNi_{3/4}Mo_{1/4}O_3$ (a) and $LaNi_{3/4}W_{1/4}O_3$ (b) at various temperatures. Solid lines are the fitting of the Jonscher's power law.

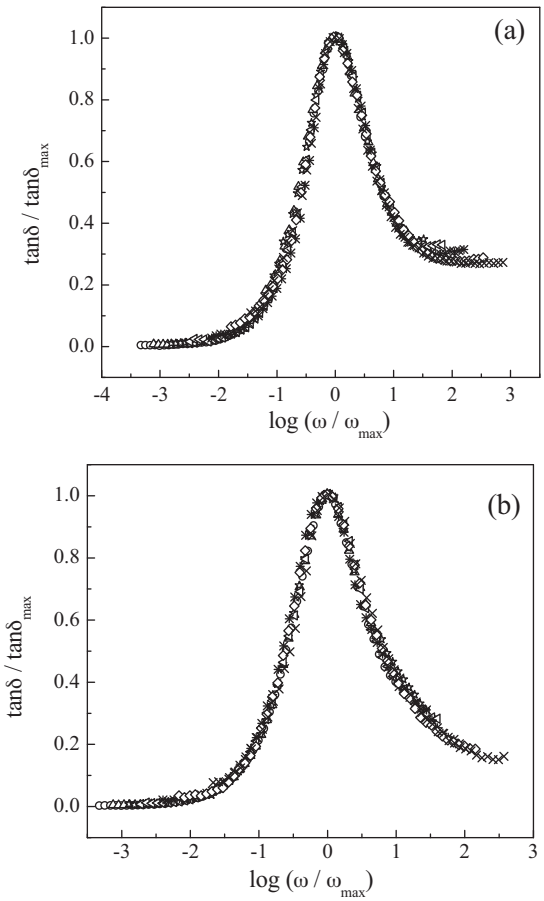

Fig. 10. Scaling behaviour of tan δ for $LaNi_{3/4}Mo_{1/4}O_3$ (a) and $LaNi_{3/4}W_{1/4}O_3$ (b).

0.054 eV respectively. It is observed from the above analysis that the band gap energy as well as activation energy of the hopping of charge carriers is high in LNW with respect to LNM. It is well known that in the perovskite oxides containing transition metal, the transport properties are mainly governed by the p–d hybridization, i.e., the interaction between the d-states of transition metal with the p-states of oxygen. This p–d hybridization is the main source of the difference of the physical quantities between the W-based material and Mo-based material though W is 5d analogue of Mo in the same column of the periodic table. Because the 5d orbital of W is more extended than the 4d orbital of Mo, the stronger 2p(O)–5d(W) hybridization pushes the 5d band, which is the antibonding state, higher in energy. Therefore, the band gap energy is high in W-based materials with respect of Mo-based material. Since, the band gap is large in LNW the required activation energy for the charge transport between the valence band and conduction band is also high according to the basic concept of semiconducting materials.

The frequency spectra of the ac conductivity for LNM and LNW are shown in Figs. 9(a) and (b) respectively. The very basic fact about ac conductivity in complex perovskite oxides is that conductivity σ is an increasing function of frequency (any hopping model has this feature). The conductivity shows a dispersion which shifts to higher frequency side with the increase of temperature. It is seen from Fig. 9 that σ decreases with decreasing frequency and becomes independent of frequency after a certain value. This part of ac conductivity represents the long range motion of the charge carriers as like as in the case of dc conductivity. The real part of ac conductivity spectra can be explained by the Jonscher's power law [36,37] and the best fits of the conductivity spectra are shown in Fig. 9 by solid lines.

Fig. 10 shows the scaling behaviour of tan δ where we have scaled each tan δ by tan δ_{max} and each frequency by ω_{max} (peak frequency of tan δ). The overlap of the curves for all the temperatures into a single master curve indicates that relaxation describes the same mechanism at different temperatures in these materials.

4. Conclusion

In order to investigate the electrical transport in LNM and LNW, the conductivity and dielectric properties in these polycrystalline materials are investigated in the temperature range from 163 K to 383 K and frequency range from 50 Hz to 1 MHz. The X-ray diffraction patterns of the samples show monoclinic phase at room temperature. The homogeneity of the samples is determined by energy dispersive analysis of X-ray attached with a scanning electron microscope. The temperature dependence of dc conductivity shows the semiconducting nature of the materials. The increase of the peak value of the loss tangent as well as the shifting of the peak position to the higher frequency side with increasing temperature indicates the polaronic transport in these materials. The complex impedance plane plots show that the relaxation (conduction) mechanism in these materials is purely a bulk effect arising from the semiconductive grains. The frequency-dependent electrical data are also analyzed in the framework of conductivity formalism. The conductivity spectra follow the universal power law. The activation energy required for bulk conduction is 0.143 eV and 0.165 eV for LNM and LNW respectively. The band gap energy of LNW is higher than the LNM due to the strong p–d hybridization in LNW with respect to LNM. The scaling behaviour of tan δ suggests that the relaxation describes the same mechanism at various temperatures.

Acknowledgements

This work is financially supported by Department of Science and Technology of India under grant no. SR/S2/CMP-01/2008. Alo Dutta acknowledges the financial support provided by the CSIR, New Delhi in the form of SRF (extended).

References

[1] R.J. Cava, J. Mater. Chem. 11 (2001) 54–62.
[2] S. Komine, Physica B 392 (2007) 348–352.
[3] E. Iguchi, K.J. Lee, J. Mater. Sci. 28 (1993) 5809–5813.
[4] N. Ortega, A. Kumar, P. Bhattacharya, S.B. Majumder, R.S. Katiyar, Phys. Rev. B 77 (2008), 014111-1–10.
[5] R.N.P. Choudhary, K. Dillip, C.M. Pradhan, G.E. Tirado, R.S. Bonilla, Katiyar, Physica B 393 (2007) 24–31.
[6] A.S. Alexandrov, N.F. Mott, Polarons and Bipolarons, World Scientific, Singapore, 1995.
[7] G.D. Mahan, Many Particle Physics, Plenum, New York, 1996.
[8] J.T. Devrcese, in: G.L. Trigg (Ed.), Encyclopedia of Applied Physics, vol. 14, VCH, New York, 1996, p. 383.
[9] E. Iguchi, N. Kubota, T. Nakamori, N. Yamamoto, K.J. Lee, Phys. Rev. B 43 (1991) 8646–8649.
[10] T. Arima, Y. Tokura, Phys. Rev. B 48 (1993) 17006–17009.
[11] C.N.R. Rao, O.M. Prakash, P. Gunguly, J. Solid State Chem. 15 (1975) 186–192.
[12] H. Takahashi, F. Munakata, M. Yamanaka, Phys. Rev. B 53 (1996) 3731–3740.
[13] S. Yamaguti, Y. Okimoto, H. Taniguti, Y. Tokura, Phys. Rev. B 53 (1996) R2926–R2929.
[14] A. Chainani, M. Marhew, D.D. Sarma, Phys. Rev. B 46 (1992) 9976–9983.
[15] E. Iguchi, W.H. Jung, J. Phys. Soc. Jpn. 63 (1994) 3078–3086.
[16] K.J. Lee, A. Iguchi, E. Iguchi, J. Phys. Chem. Solids 54 (1993) 975–981.
[17] E. Iguchi, K. Ueda, W.H. Jung, Phys. Rev. B 54 (1996) 17431–17437.
[18] W.H. Jung, J. Appl. Phys. 90 (2001) 2455–2458.
[19] S. Komine, E. Iguchi, J. Phys. Chem. Solids 68 (2007) 1504–1507.
[20] A. Dutta, T.P. Sinha, S. Shannigrahi, Phys. Rev. B 76 (2007), 155113-1–7.
[21] A. Dutta, T.P. Sinha, S. Shannigrahi, J. Appl. Phys. 104 (2008), 064114-1–6.
[22] Sonali Saha, T.P. Sinha, J. Appl. Phys. 99 (2006), 014109-1–5.
[23] A. Dutta, T.P. Sinha, J. Phys. Chem. Solids 67 (2006) 1484–1491.
[24] S. Komine, E. Iguchi, J. Phys.: Condens. Matter 16 (2004) 1061–1074.
[25] A.R. Long, in: M. Pollak, B. Shklovskii (Eds.), Hopping Transport in Solids, North-Holland, Amsterdam, 1991, p. 207.

[26] P. Debye, Polar Molecules, Chemical Catalogue Company, New York, 1929.
[27] E. Iguchi, K. Akashi, J. Phys. Soc. Jpn. 61 (1992) 3385–3393.
[28] I.G. Austin, N.F. Mott, Adv. Phys. 18 (1969) 41–102.
[29] T. Holstein, Ann. Phys. (N. Y.) 8 (1959) 343–389.
[30] F.P. Koffyberg, F.A. Banko, J. Non Cryst. Solids 40 (1980) 7–17.
[31] W.H. Jung, E. Iguchi, J. Phys.: Condens. Matter 7 (1995) 1215–1227.
[32] W.H. Jung, E. Iguchi, Philos. Mag. B 73 (1996) 873–891.
[33] E. Iguchi, N. Nakamura, J. Phys. Chem. Solids 58 (1997) 755–763.
[34] L.A.K. Dominik, R.K. MacCrone, Phys. Rev. 163 (1967) 756–768.
[35] W.H. Jung, H. Nakatsugawa, E. Iguchi, J. Solid State Chem. 133 (1997) 466–472.
[36] A.K. Jonscher, J. Phys. D: Appl. Phys. 13 (1980) L89–L94.
[37] A.K. Jonscher, Dielectric Relaxation in Solids, Chelsea Dielectrics Press, London, 1983.